Supplementary Information:

# Electronic Structure and Chemical Nature of Oxygen Dopant States in Carbon Nanotubes

Xuedan Ma[1], Lyudmyla Adamska[2], Hisato Yamaguchi[1], Sibel Ebru Yalcin[1], Sergei Tretiak[1,2], Stephen K. Doorn[1*], and Han Htoon[1*]

[1]Center for Integrated Nanotechnologies, Materials Physics and Applications Division, [2]Theory Division, Los Alamos National Laboratory, New Mexico, 87545, USA

This document contains the following supplementary information:

**S1 PL Characteristics of undoped and oxygen-doped SWCNTs**

At room temperature PL images of both undoped and oxygen doped SWCNTs show elongated images (Fig. S1a, c). FWHM values of tube PL intensity profiles perpendicular to tube axes at room temperature (~ 400 nm) and low temperature (~ 1.1 μm) are consistent with the diffraction limit of our imaging system. FWHM values of tube PL intensity profiles along the tube axes give a good estimate of the tube lengths. The estimated lengths are distributed between 0.6 to 6 μm. Only diffraction limited spots were observed in low T PL images of both undoped and doped tubes, suggesting that PL originates from excitons localized in less than 400 nm regions of the tubes at low T. Weak potential fluctuations that exist along the length of the SWCNTs might be responsible for this localization.

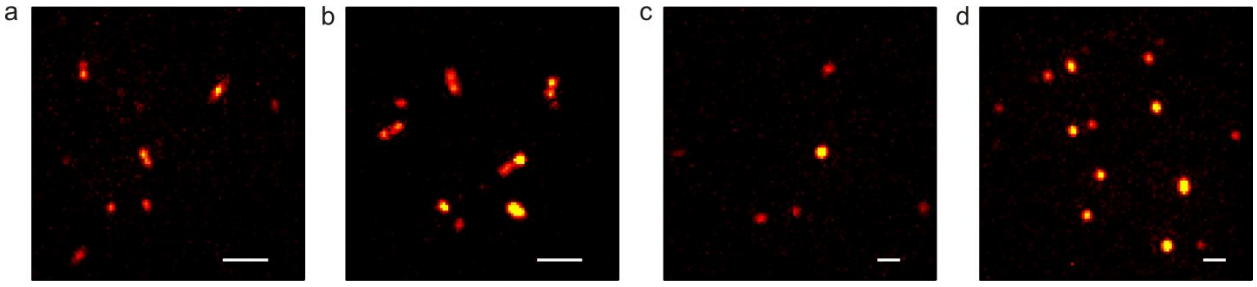


Figure S1. PL images of undoped (a, c) and oxygen doped (b, d) SWCNTs at room temperature (a, b) and 4 K (c, d). Scale bar is 5 μm.

PL spectra of most individual undoped SWCNTs (Fig. S2a) can be fitted with single Lorentzian functions (Fig. S2a, Inset). A majority of the tubes show stable PL intensity and are nearly free of PL blinking and spectral diffusion (Fig. S2b). Fig. S2c and S2d show histograms of the fitting results for peak positions (Fig. S2c) and FWHM values (Fig. S2d). The position and FWHM distributions have means of 1.251 eV and 4.40 meV with standard deviations of 0.005 eV and 0.008 meV, respectively.

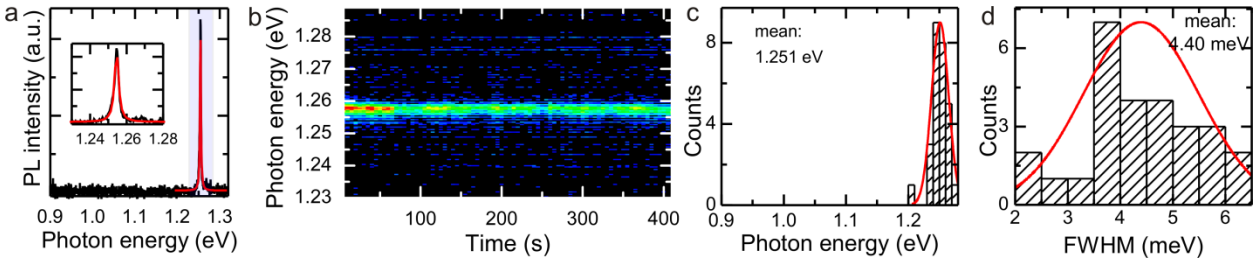


Figure S2. a, A PL spectrum of an undoped (6,5) SWCNT (black) together with a Lorentzian fitting curve (red). The integration time was 20s. The inset shows an enlarged view of the shadowed area. b, A contour plot of the temporal evolution of the PL spectrum of the undoped (6,5) SWCNT shown in a. The integration time per spectrum was 5s. c, d, Histograms of peak positions (c) and FWHM values (d) of the Lorentzian functions used to fit PL spectra of individual undoped SWCNTs. The fitting curves (red) are Gaussian functions.

$E_{11}^{+}$, $E_{11}$, and $E_{11}^{-}$ peaks of oxygen-doped SWCNTs can also be fitted with Lorentzian functions. Fig. S3a and S3b show the histograms of peak position and FWHM results from Lorentzian fitting. While the mean of the peak position distribution (1.244 eV) (Fig. S3a) is essentially the same as that for undoped tubes, the mean of the FWHM distributions 5.30 meV ± 0.01 meV (Fig. S3b) is slightly broader than that for the undoped species.

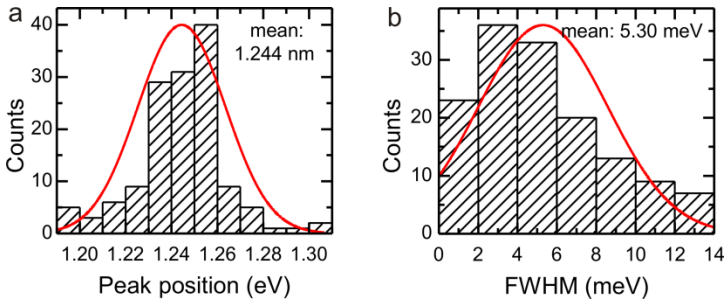


Figure S3. Histograms of peak positions (a) and FWHM values (b) of the Lorentzian functions used to fit $E_{11}^{+}$, $E_{11}$, and $E_{11}^{-}$ peaks of individual oxygen-doped SWCNTs. The fitting curves (red) are Gaussian functions.

**S2 PL spectra of oxygen-doped SWCNTs excited by a 561 nm laser**

To test if the spectral splitting at ~1.25 eV in oxygen-doped SWCNTs is due to Raman peaks, a 561 nm continuous-wave laser is used to excite the tubes at their $E_{22}$ resonance, because if the new peaks are Raman peaks, they should not be observed at the same energy by two different excitation wavelengths (820 nm and 561 nm). Example PL spectra of three individual oxygen-doped SWCNTs are shown in Fig. S4, and one (Fig. S4a), two (Fig. S4b) and three (Fig. S4c) peak(s) at around 1.25 eV can be observed. Therefore, we exclude the possibility of Raman peaks.

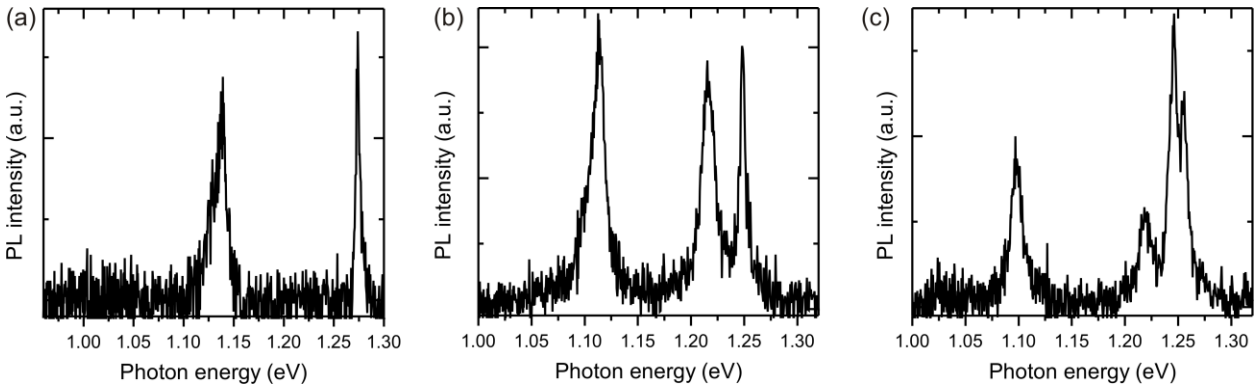


Figure S4. PL spectra of three representative oxygen-doped SWCNTs excited at 561 nm. Splitting in the $E_{11}$ peaks can be observed in (b) and (c).

**S3 Position and linewidth of the PL peaks at ~ 1.10 eV in oxygen-doped SWCNTs**

Fig. S5a shows a histogram of peak positions of the peaks at ~ 1.10 eV in oxygen-doped SWCNTs. The histogram can be fitted by three Gaussian functions centered at 0.991 eV ($E_{11}^{*-}$, peak), 1.112 eV ($E_{11}^{*}$, peak), and 1.180 eV ($E_{11}^{*+}$, peak). Fig. S5b shows the FWHM of the peaks with an average value of 6.38 meV.

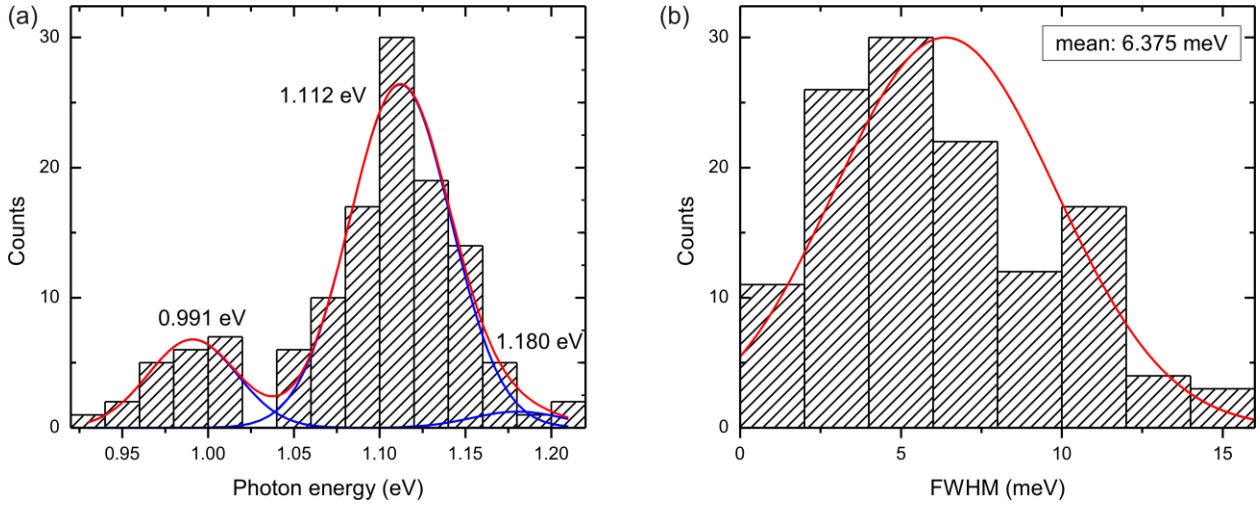


Figure S5. (a) A histogram of the positions of the PL peaks at ~ 1.10 eV in oxygen-doped SWCNTs. Fitting the histogram with Gaussian functions (blue curves) gives three peaks at 1.180 eV, 1.112 eV, and 0.991 eV. (b) A histogram of the FWHM of the peaks in oxygen-doped SWCNTs. The average width is 6.38 meV.

**S4 PL Fluctuations of Deep Trap States**

Fig. S6a displays a complete data set for the PL intensity correlation shown in Fig. 2e of the main text. PL intensities of the $E_{11}$, and $E_{11}^{*}$, peaks (y-axes) are plotted against the PL intensity of the $E_{11}^{-}$ peak to extract the degree of correlation in Fig. S6b and S6c, respectively. Correlations calculated from these intensities using the Pearson product-moment correlation

coefficient ($r_{xy} = \frac{n\sum x_i y_i - \sum x_i \sum y_i}{\sqrt{n\sum x_i^2 - (\sum x_i)^2}\sqrt{n\sum y_i^2 - (\sum y_i)^2}}$) yields a positive correlation coefficient of 0.70 for Fig. S6b and a negative correlation coefficient of -0.21 for Fig. S6c. Fig S7 displays two additional examples of intensity correlations between the different PL peaks in oxygen-doped SWCNTs. Here we note that observation of positive/negative PL correlations requires CCD integration time to coincide with the fluctuation time of exciton trapping efficiency discussed in the main text. In addition to this modulation of exciton trapping efficiency, PL fluctuations of doped SWCNTs can also be controlled by other environmental factors that control the PL fluctuations of undoped SWCNTs. Because of these factors, the positive/negative PL correlations demonstrated here in Fig. S6 and S7 were observed only in a small fraction of the SWCNTs.

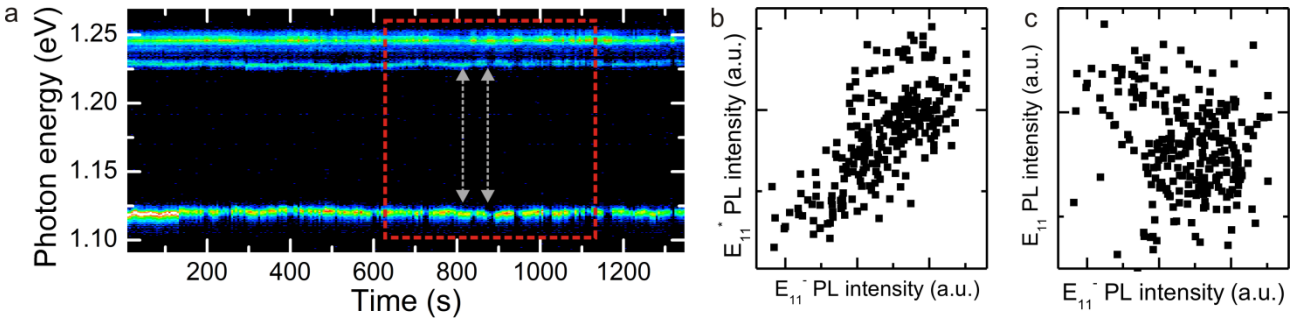


Figure S6. A complete data set of temporal evolution of PL spectra shown in Figure 2e in the main text. b, c, PL intensity correlations between the $E_{11}^{-}$, and $E_{11}^{*}$, peaks (b), and $E_{11}^{-}$ and $E_{11}$ peaks (c), corresponding to positive and negative correlation coefficients of 0.70 and -0.21, respectively.

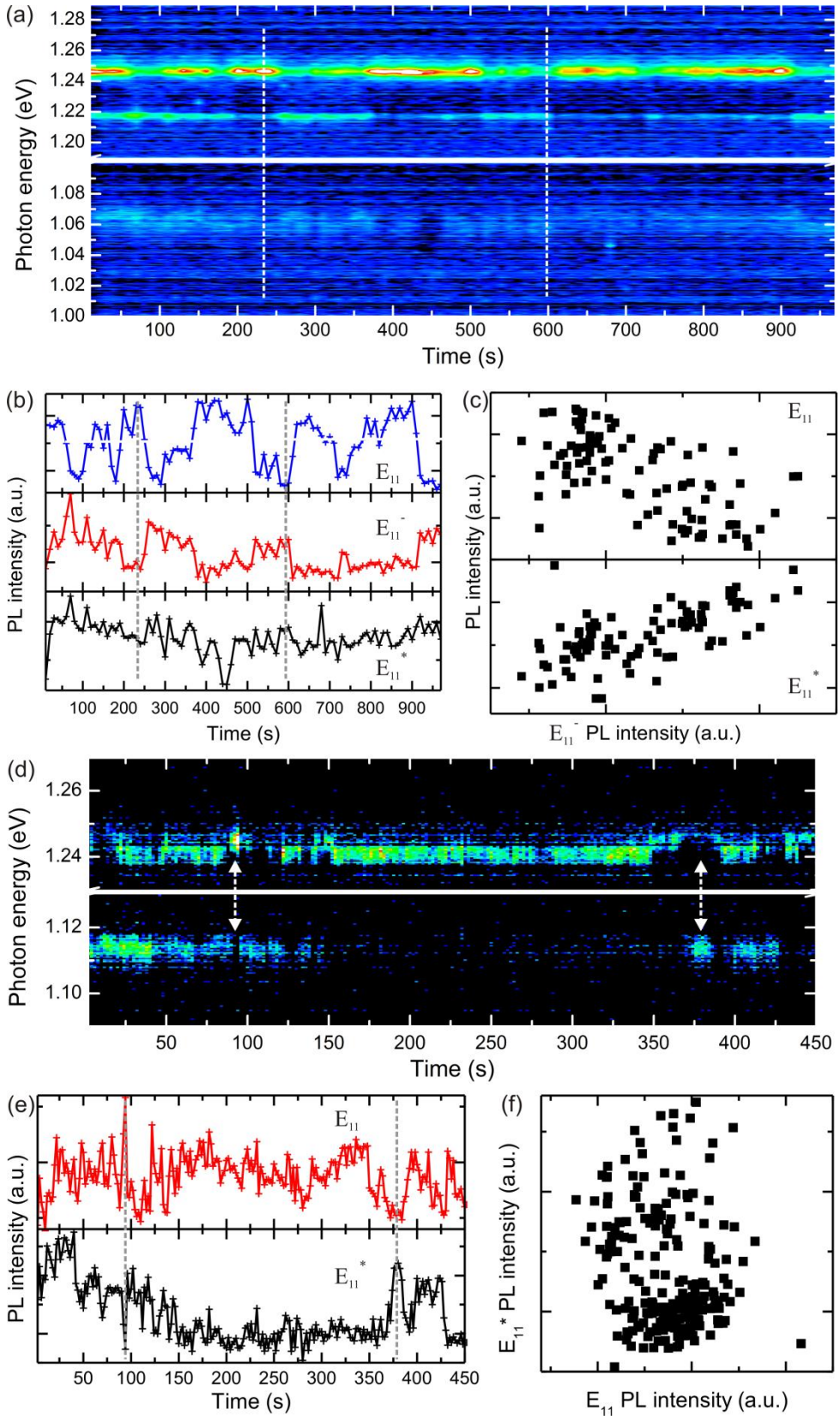
(a)
Photon energy (eV)
1.28
1.26
1.24
1.22
1.20
1.08
1.06
1.04
1.02
1.00
100
200
300
400
500
600
700
800
900
Time (s)
(b)
PL intensity (a.u.)
E11
E11-
E11*
100 200 300 400 500 600 700 800 900
Time (s)
(c)
PL intensity (a.u.)
E11
E11*
E11- PL intensity (a.u.)
(d)
Photon energy (eV)
1.26
1.24
1.12
1.10
50
100
150
200
250
300
350
400
450
Time (s)
(e)
PL intensity (a.u.)
E11
E11*
50 100 150 200 250 300 350 400 450
Time (s)
(f)
E11* PL intensity (a.u.)
E11 PL intensity (a.u.)

Figure S7. Two more examples (a-c and d-f) of negative PL correlations between the $E_{11}$ peak, the $E_{11}^{-}$ and $E_{11}^{*}$ peaks in oxygen-doped SWCNTs.

**S5 Computation of electronic properties of undoped and oxygen-doped (6,5) SWCNTs**

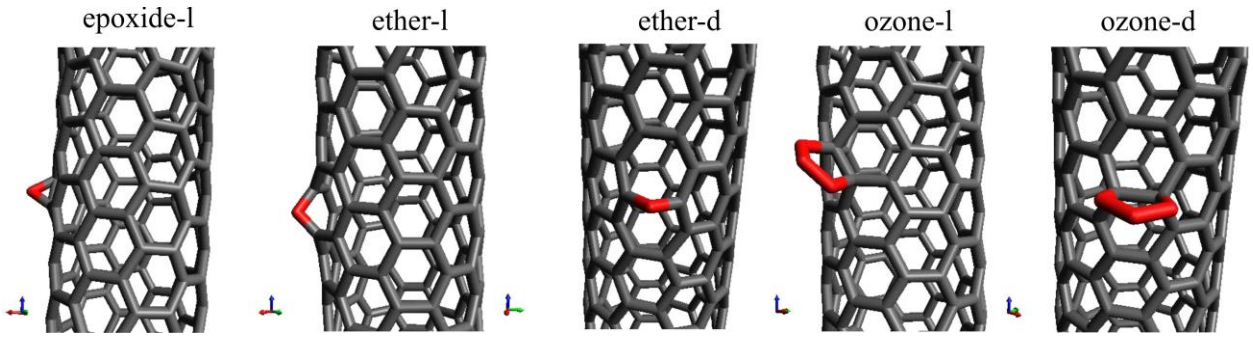


Figure S8. Optimal atomic structures of an 8 nm long (6,5) SWCNT with different functional groups/molecules.

Table S1 Binding energies, formation energies and band gaps of different adducts of SWCNTs

| Structure | Binding energy (eV) | Formation energy (eV) | HOMO (eV) | LUMO (eV) | Band gap (eV) |
|---|---|---|---|---|---|
| undoped | | | -2.87 | -1.11 | 1.76 |
| epoxide-l | -3.75 | + | -2.81 | -1.30 | 1.51 |
| ether-l | -2.81 | + | -2.88 | -1.11 | 1.77 |
| ether-d | -5.28 | -0.17 | -2.86 | -1.16 | 1.70 |
| ozone-l | +0.66 | + | -2.42 | -1.39 | 1.03 |

| | | | | | |
|---|---|---|---|---|---|
| ozone-d | +0.75 | + | -2.40 | -1.23 | 1.17 |

**S6 Exciton distribution in undoped and oxygen-doped SWCNTs**

As already mentioned in section S5, transition densities, which represent real space exciton distributions, in undoped and oxygen-doped (6,5) SWCNTs have been calculated using a single-point-energy run with Gaussian 09 TDDFT at the B3LYP/STO-3G level of the theory. Following the sequence of absorption peaks in Fig. 1g (lower panel) in the main text, transition densities of different energetic states in undoped and epoxide-l, ether-d, and ether-l adducts of (6,5) SWCNTs are plotted in Fig. S9. For the excitons with energy shifts smaller than 50 meV, which correspond to the $E_{11}^{-}$, $E_{11,}$ and $E_{11}^{+}$ peaks, delocalization of the exciton along the tube can be clearly observed. However, for the excitons with energy shifts larger than 50 meV, which correspond to the $E_{11}^{*-}$, $E_{11}^{*}$, and $E_{11}^{*+}$ peaks, clear localization of excitons at the doping site can be observed for most excitons (except for epoxide-l at 54 meV).

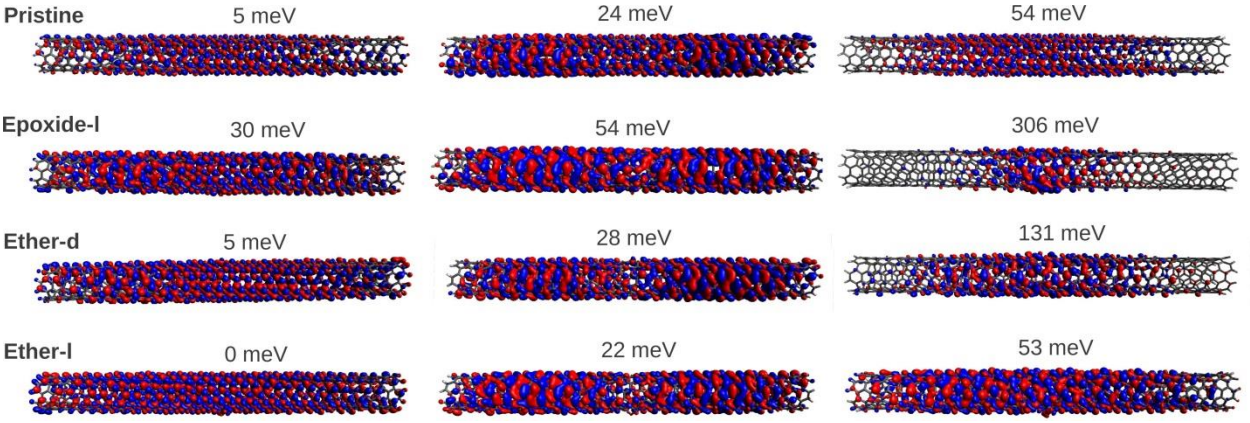


Figure S9. Transition densities of different electronic states in undoped and epoxide-l, ether-d, and ether-l adducts of (6,5) SWCNTs. Red and blue dots represent electrons and holes, respectively.

While excitons of the higher energy states with energy shifts <50meV are delocalized over the entire tube length, those of the lowest energy trap states (i.e. $E_{11}^{*}$ and $E_{11}^{*-}$ at ether-d,131 meV and epoxide-l 306 meV) are spatially localized and pinned to 3-4 nm regions of the respective dopant sites.

**S7 Additional PL saturation data**

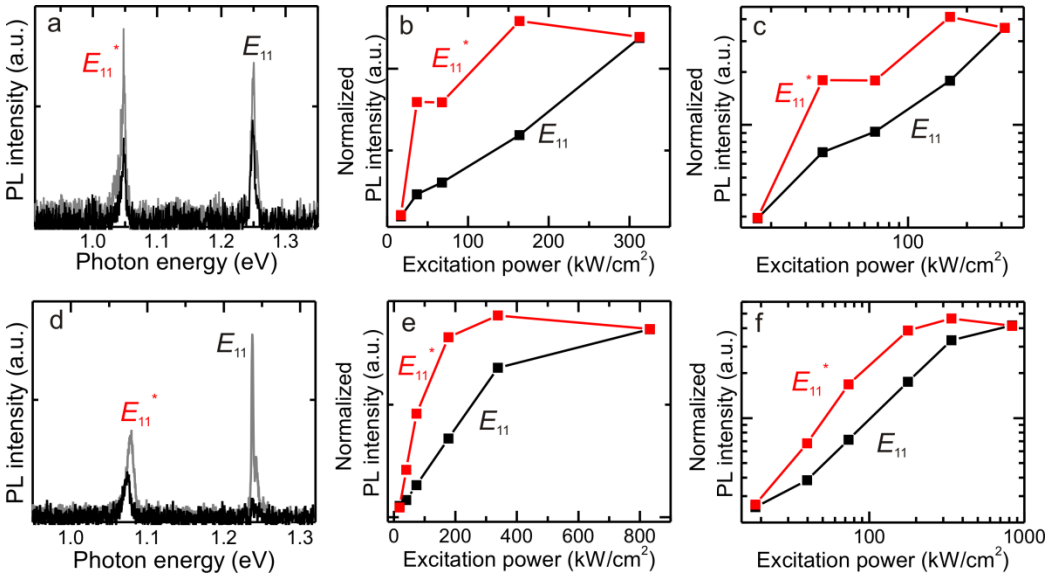


Figure S10. (a, d) Low T PL spectra of two oxygen doped tubes. (b,e) PL saturation behavior of $E_{11}$ (black) and $E_{11}^{*}$ (red) peaks plotted in linear-linear plot. (c,f) (b) and (e) redisplayed as log-log plots.

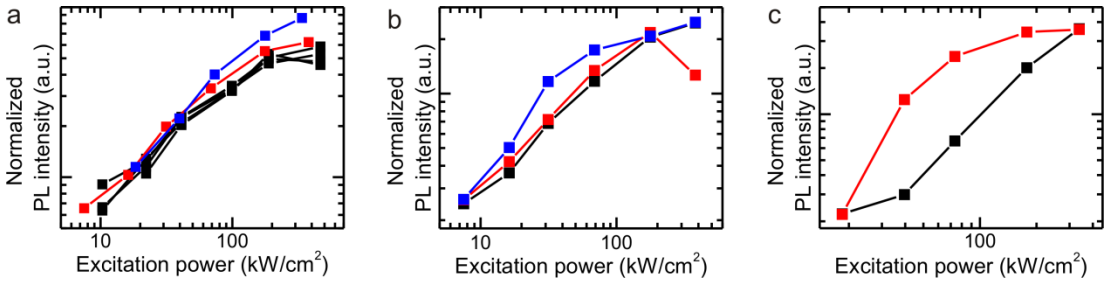


Figure S11. Fig. 4b, 4d and 4f of the main text redisplayed as log-log plots in (a), (b), and (c), respectively.